

*Invited Paper*

# Gyro-devices – natural sources of high-power high-order angular momentum millimeter-wave beams

M. Thumm<sup>1,2\*</sup>

Karlsruhe Institute of Technology (KIT), Kaiserstr. 12, 76131 Karlsruhe, Germany

<sup>1</sup> Institute for Pulsed Power and Microwave Technology (IHM)<sup>2</sup> Institute of Radiofrequency Engineering and Electronics (IHE)

\* Email: manfred.thumm@kit.edu

(Received January 23, 2020)

**Abstract:** The Orbital Angular Momentum (OAM) carried by light beams with helical phasefront (vortex beams) has been widely employed in many applications such as optical tweezers, optical drives of micro-machines, atom trapping, and optical communication. OAM provides an additional dimension (diversity) to multiplexing techniques, which can be utilized in addition to conventional multiplexing methods to achieve higher data rates in wireless communication. OAM beams have been thoroughly studied and used in the optical regime but in the mm-wave and THz-wave region, they are still under investigation. In these frequency bands, there are difficulties associated with beam-splitting and beam-combining processes as well as with the use of spiral phase plates and other methods for OAM generation, since the wavelength is much larger compared to those at optical frequencies, leading to higher diffraction losses.

The present paper describes the natural generation of high-power OAM modes by gyro-type vacuum electron devices with cylindrical interaction circuit and axial output of the generated rotating higher-order transverse electric mode  $TE_{m,n}$ , where  $m > 1$  and  $n$  are the azimuthal and radial mode index, respectively. The ratio between the total angular momentum (TAM)  $J_N$  and total energy  $W_N$  of  $N$  photons is given by  $m/\omega$ , where  $\omega$  is the angular frequency of the operating mode, which in a gyrotron oscillator is close to the  $TE_{m,n}$ -mode cutoff frequency in the cavity. Therefore,  $m/\omega = R_c/c$ , where  $R_c$  is the caustic radius and  $c$  the velocity of light in vacuum. This means that the OAM is proportional to the caustic radius and at a given frequency the same for all modes with the same azimuthal index  $m$ . Right-hand rotation (co-rotation with the electrons) corresponds to a positive value of  $m$  and left-hand rotation to negative  $m$ . The corresponding OAM mode number (topological charge) is  $l = m - 1$ . Circularly polarized  $TE_{1n}$  modes only possess a Spin Angular Momentum (SAM:  $s = \pm 1$ ).  $TE_{0n}$  modes have neither SAM nor OAM.

This is the result of the photonic (quasi-optical) approach to derive the TAM of modes generated in gyrotrons. The same result follows from the electromagnetic (EM) wave approach for the TAM within a given waveguide volume per total energy of the EM wave in the same volume.

Such high-power output beams with very pure higher-order OAM, generated by gyrotron oscillators or amplifiers (broadband) could be used for multiplexing in long-range wireless communications. The corresponding mode and helical wavefront sensitive detectors for selective OAM-mode sorting are available and described in the present paper.

**Keywords:** Orbital angular momentum (OAM), Spin angular momentum (SAM), Millimeter-wave and THz-wave vortex beams, Gyrotron, Gyro-amplifiers, Long-range wireless communication, Multiplexing, Diversity.

## 1. Introduction

Electromagnetic (EM) waves carry linear and angular momentum [1]. The linear momentum is associated with the Poynting vector  $\vec{S}$ , which represents the directional energy flux (the energy transfer per unit area per unit time, measured in  $W/m^2$ ). The total angular momentum (TAM) of paraxial EM wave beams can be described as the sum of spin angular momentum (SAM) and orbital angular momentum (OAM), where the SAM is associated with the polarization state [2, 3]. The SAM per photon is given by  $s \cdot \hbar$ , where  $\hbar$  is the Planck constant divided by  $2\pi$  and  $-1 \leq s \leq 1$ . SAM-state  $s = 0$  corresponds to linear polarization and  $s = \pm 1$  to right-handed circular polarization (RHCP) and left-handed circular polarization (LHCP), respectively. In between, the wave beam is elliptically polarized. The OAM is related to the spatial wave front with the azimuthal phase distribution  $\exp(-jl\phi)$ , where  $\phi$  is the azimuthal angle and  $l$  is any integer, the so-called topological charge or OAM state number [4]. The OAM per photon is given by  $l \cdot \hbar$ , with positive  $l$  for right-handed and negative  $l$  for left-handed phase rotation. EM wave beams carrying OAM (often called vortex beams) exhibit unique features like azimuthal phase changes in a plane perpendicular to the beam axis (helical phase fronts) and an amplitude singularity (annular doughnut shape) in the propagation direction. The amount of phase front twisting is determined by the OAM state number  $l$  ( $|l|$  phase spirals). EM wave beams with different OAM are mutually orthogonal, allowing them to be multiplexed together at the same carrier frequency along the same propagation axis and de-multiplexed with low crosstalk. Therefore, in addition to conventional multiplexing methods to achieve higher data rates, OAM can be an effective means to increase the channel capacity and spectral efficiency in wireless communication technology by a factor equal to the number of available OAM states (OAM diversity) [5].

OAM beams have been thoroughly studied and used in the optical regime for high-speed, terabit OAM multiplexing wireless communications [5] and in the areas of sensitive optical detection, orientational manipulation (optical tweezers), optical drives of micro-machines, atom trapping, quantum information processing and biology microscopy [6, 7].

Despite the various applications of OAM, it is still a challenging task to generate OAM beams with pure and controllable topological charge state  $l$ . Many methods have been developed to realize such OAM modes, including spiral phase plates (SPPs), holographic diffraction gratings (pitch-fork hologram), birefringent liquid crystals (Q-plate), spiral reflectors, specific array antennas, and anisotropic frequency selective surfaces (meta-surfaces) [8, 9, and references given there]. In the microwave and mm-wave region there are difficulties associated with diffraction losses since the wavelength is much larger compared to those at optical frequencies. Reviews on the state-of-the-art and applications in this frequency region are given in [10, 11]. Record values in high-capacity mm-wave communications with OAM multiplexing have been reported in [12]. In this article eight multiplexed 28 GHz OAM beams ( $l = \pm 1$  and  $\pm 3$  on each of two orthogonal

polarizations), generated by SPPs, each carrying a 4x1 Gbit/s (4 *bits* per symbol) quadrature amplitude modulation (16-QAM) signal, thereby achieving a capacity of 32 *Gbit/s*, were transmitted over a distance of 2.5 *m* with a spectral efficiency of  $\approx 16 \text{ bit}/(\text{s}\cdot\text{Hz})$ . All the eight OAM channels were recovered with bit-error rates (*BERs*) below  $3.8 \times 10^{-3}$ .

The present paper shows that gyrotron oscillators and gyro-amplifiers are natural sources of high-power mm-wave beams with very pure higher-order OAM, which can be used for multiplexing in long-range wireless communication. The corresponding mode and helical wavefront sensitive detectors for selective OAM-mode sorting are available and also described in this report. Section 2 gives an overview on gyro-devices and their interaction principles. The OAM and SAM characteristics of rotating gyrotron cavity modes are discussed in Section 3. Section 4 shows examples of high-power, high-order gyrotron OAM beam transmitters and Section 5 introduces to corresponding mode and helical wavefront selective receivers for OAM mode sorting. Finally, Section 6 gives the conclusions and summarizes the present results.

## 2. Gyro-devices

Gyro-devices are electron cyclotron masers in which electromagnetic (EM) waves with the angular frequency  $\omega$  are generated by relativistic electrons gyrating in an external longitudinal magnetic field with a perpendicular velocity  $v_{\perp}$  [13]. The resonance condition between the periodic rotation of the electrons and the EM wave (TE mode) in the interaction circuit is

$$\omega - k_{\parallel} v_{\parallel} = q\Omega_c, \quad q = 1, 2, \dots, \quad (1)$$

where  $k_{\parallel}$  is the characteristic axial wavenumber of the EM wave in the interaction structure,  $v_{\parallel}$  is the longitudinal electron drift velocity and  $\Omega_c = \Omega_{co}/\gamma$  is the relativistic electron cyclotron frequency.

The non-relativistic electron cyclotron frequency  $\Omega_{co}$  is given by

$$\Omega_{co}(r) = eB/m_o \quad (2)$$

where  $e$  and  $m_o$  are the electrical charge and rest mass of an electron and  $B$  is the magnitude of the cavity magnetic field. The relativistic Lorentz factor  $\gamma$  can be simply calculated from

$$\gamma = 1 + eV_b / m_o c^2 \approx 1 + V_b / 511, \quad (3)$$

where  $c$  is the free-space velocity of light and  $V_b$  the acceleration voltage of the electron beam in kV. In the present paper, the field vector  $\vec{B}$  is pointing to the output of the interaction circuit.

Gyrotrons are oscillators, which mainly employ weakly relativistic electron beams ( $V_b \leq 80$  kV,  $\gamma \leq 1.16$ ) with high transverse momentum (velocity ratio  $\alpha = v_{\perp}/v_{\parallel} = 1.2-1.5$ ) [13, 14]. The wave vector of the EM wave in the cavity is almost transverse to the direction of the longitudinal magnetic field ( $k_{\perp} \gg k_{\parallel}$  and the Doppler shift is small), resulting, according to eq. (1), in wave generation near the electron cyclotron frequency or one of its harmonics:

$$\omega \cong q\Omega_c, \quad q = 1, 2, \dots \quad (4)$$

In gyrotrons with cylindrical waveguide cavity, the operating  $TE_{m,n}$  mode is close to cutoff, which means  $v_{ph} = \omega/k_z \gg c$  and the frequency mismatch  $\omega - q\Omega_c$  is small but positive in order to achieve correct phasing, i.e. keeping the azimuthal electron bunches in the retarding phase to transfer energy to the TE wave. The Doppler term  $k_{\parallel}v_{\parallel}$  is of the order of the gain width and is small compared to the radiation frequency.

The frequency of a gyrotron is approximately given by the cutoff frequency  $f_{cut}$  of the cavity mode [15]:

$$f_{cut} \text{ (GHz)} = 95.4269 \chi_{m,n} / D \text{ (mm)} \quad (5)$$

where  $\chi_{m,n}$  is the  $n^{\text{th}}$  root of the derivative of the corresponding Bessel function  $J'_m$  ( $TE_{mn}$  mode) and  $D = 2R_0$  is the cavity diameter.

Gyrotrons, as fast-wave devices with  $v_{ph} > c$ , are capable of producing very high-power radiation at cm, mm and sub-mm wavelengths [13, 14], since the use of large cavity and output waveguide cross sections reduces wall losses as well as the danger of breakdown and permits the passage of large, high-power electron beams. In contrast to klystrons, the resonance frequency of a gyrotron cavity is not determined by the characteristic cavity size, but by the strength of the magnetic field (see eqs. (1) and (3)). Then, according to eq. (5) for a given frequency, operation in a rotating high-order mode (determined by its eigenvalue  $\chi_{m,n}$ ) with low Ohmic attenuation can be selected just by the cavity radius  $R_0$ . Operation at the  $q^{\text{th}}$  cyclotron harmonic frequency reduces the required magnetic field for a given frequency by the factor  $q$ .

Whether the direction of cavity mode rotation is co- or counter with respect to the electron gyration in the cavity magnetic field  $\vec{B}$  depends on the positioning of the annular electron beam. If the electron beam radius  $R_b$  for fundamental frequency excitation ( $q = 1$ ) is chosen as [15]

$$R_b = \chi_{m-1,l} R_0 / \chi_{m,n} \quad (6)$$

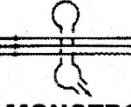

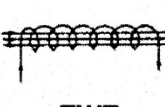
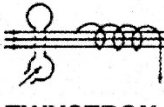
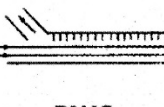


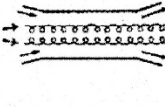
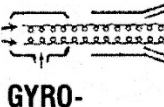
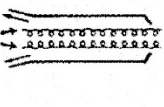
the generated  $TE_{m,n}$  mode is co-rotating (right-hand rotating), and for

$$R_b = \chi_{m+1,l} R_0 / \chi_{m,n} \quad (7)$$

it is counter-rotating (left-hand rotation). The corresponding beam radii are a little bit smaller and a little bit larger than the radius of the intensity maximum of the cavity  $TE_{m,n}$  mode. In the case of the circular symmetric  $TE_{0,n}$  modes both radii are the same and identical with the radius of the maximum of the electric field. There is no mode rotation. In the case of  $TE_{m,l}$  modes, only the co-rotating modes can be excited, since always  $\chi_{m+1,l} > \chi_{m,l}$  (therefore, according to (7):  $R_b > R_0$ !).

Bunching of electrons in gyro-devices has much in common with that in conventional linear electron beam devices, namely, monotron, klystron, TWT, twystron and BWO [13]. In both cases the primary energy modulation of electrons gives rise to bunching (azimuthal or longitudinal), which is inertial. The bunching continues even after the primary modulation field is switched off (in the drift sections of klystron-type and twystron-type devices). This analogy suggests the correspondence between conventional linear-beam (O-type) devices and various types of gyro-devices. Table 1 presents the schematic drawings of devices of both classes [14].

Tab. 1 Overview of gyro-devices and comparison with corresponding conventional linear-beam (O-type) tubes [14].

<b>"O" TYPE DEVICES</b>	 <b>MONOTRON</b>	 <b>KLYSTRON</b>	 <b>TWT</b>	 <b>TWYSTRON</b>	 <b>BWO</b>
<b>TYPE OF GYRO- DEVICE</b>	 <b>GYRO- MONOTRON</b>	 <b>GYRO- KLYSTRON</b>	 <b>GYRO-TWT</b>	 <b>GYRO- TWYSTRON</b>	 <b>GYRO BWO</b>

### 3. OAM and SAM of rotating gyrotron modes

Helically propagating rotating  $TE_{m,n}$  modes in a circular waveguide can be decomposed into a series of cylindrical plane waves, each propagating at the Brillouin angle  $\theta_B = \arcsin(\chi_{m,n}/kR_0)$  relative to the waveguide axis, where  $k = 2\pi/\lambda$  is the free-space wavenumber. The requirement of a zero azimuthal electric field at the waveguide wall defines their relative phases. In the geometric optical (g.o.) limit a plane wavefront is represented by one ray. Its transverse location is defined by the requirement that at a particular point of interest the ray direction must coincide with the direction of the Poynting vector  $\vec{S}$  of the original  $TE_{m,n}$ -mode field distribution. If the

point of interest is located at the waveguide wall the ray has the distance

$$R_c = (m/\chi_{m,n})R_0 \quad (8)$$

from the waveguide center. Hence if all plane waves are presented by g.o. rays, they form a caustic at the radius  $R_c$ . In an unperturbed circular symmetric waveguide the density of the rays along the caustic is uniform [16].

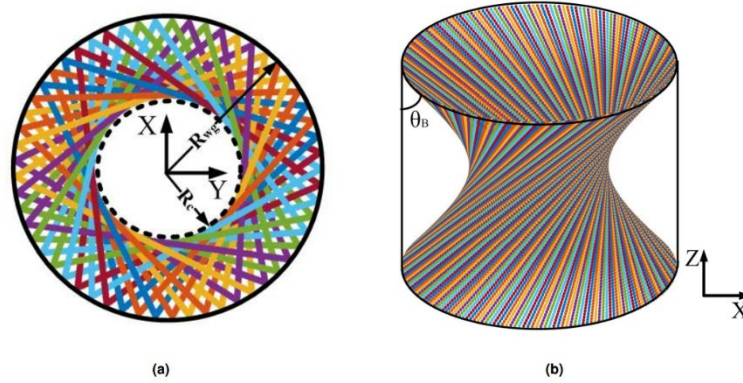


Fig.1 (a) Ray propagation for a rotating wave in a cylindrical gyrotron cavity with consecutive reflections. (b) Set of rays forming a caustic with radius  $R_c$  [16].

The total angular momentum (TAM)  $\vec{J}$  possessed by such a ray (which is tangential to the caustic of the mode) can be expressed as

$$\vec{J} = J\hat{z} = \vec{r} \times \vec{p} = R_c \hat{r} \times p_\phi \hat{\Phi} = R_c p_\phi \hat{z} \quad (9)$$

where  $p_\phi = p \sin \theta_B = \hbar k \sin \theta_B$ ,  $\sin \theta_B = \frac{k_\perp}{k}$  and  $k_\perp = \frac{\chi_{m,n}}{R_0}$ .

Therefore,

$$\vec{J} = R_c p_\phi \hat{z} = \frac{m}{\chi_{m,n}} R_0 \hbar k \frac{\chi_{m,n}}{k R_0} \hat{z} = m \hbar \hat{z} \quad (10)$$

The ratio between the magnitudes of the TAM  $J_N$  and the total energy  $W_N$  of  $N$  photons is given by

$$\frac{J_N}{W_N} = \frac{Nm\hbar}{N\hbar\omega} = \frac{m}{\omega} \quad (11)$$

where  $\omega$  is the angular frequency of the operating cavity mode, which is close to the cutoff frequency  $\omega_{cut} = c\chi_{m,n}/R_0$  in the cylindrical gyrotron cavity section. Therefore follows

$$m/\omega = R_c/c. \quad (12)$$

This is the result of the photonic (g.o.) approach [16]. Using the time averaged Poynting vector  $\vec{S}$  and the expressions of the electric and magnetic fields of rotating  $TE_{m,n}$  modes, equation (11) also follows from the EM wave approach for the TAM of a gyrotron cavity mode within a given waveguide volume per time averaged total energy of the EM wave in the same volume [16].

From relation (12), the following features of rotating gyrotron  $TE_{m,n}$  modes can be found:

- At a given frequency  $f = \omega/2\pi$ , the TAM increases with increasing azimuthal mode number  $m$ , whereas for fixed  $m$  it decreases with increasing frequency.
- At a given frequency all gyrotron modes with the same azimuthal mode number  $m$  have the same TAM (same caustic radius  $R_c$ , but different cavity radius  $R_0$ ).
- For a given gyrotron cavity radius  $R_0$ , the  $TE_{m,n}$  mode with the largest caustic radius  $R_c$  has the highest TAM. This is the co-rotating whispering gallery mode (WGM)  $TE_{m,l}$  with  $\chi_{m,l} \lesssim kR_0$ .

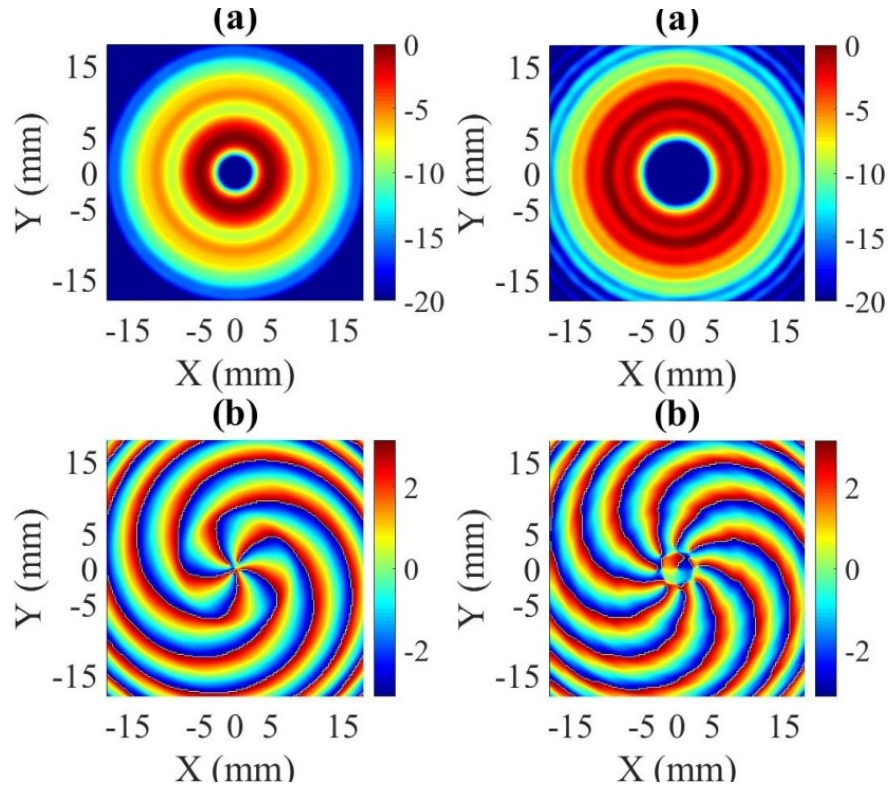


Fig. 3 Theoretical amplitude (a) and phase (b) of the time-averaged total electric field of the co-rotating 95 GHz modes  $TE_{6,2}$  (left) and  $TE_{10,1}$  (right) (in the Fresnel zone at 10 mm distance from a 20 mm diameter aperture) [17]. The propagation direction is perpendicular to the measured pattern, coming out of the plane.

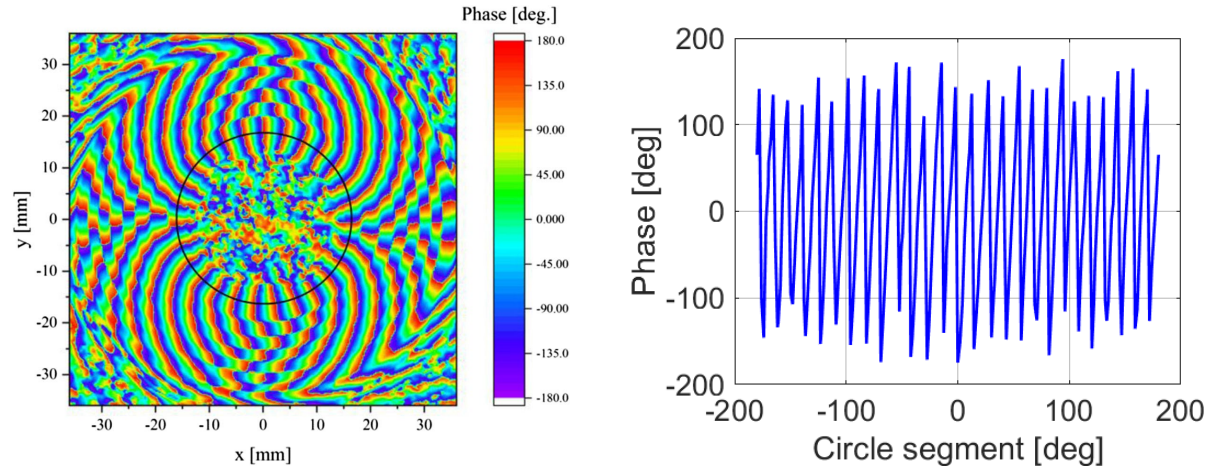


Fig. 4 Low-power (cold) measurement of 140 GHz co-rotating  $TE_{28,8}$ -mode phase pattern (left), taken with a fundamental rectangular waveguide probe for vertical polarization. Along an azimuthal circle, 27 phase spirals can be counted (right) [18].

Figure 3 shows the analytically calculated amplitude and phase of the time-averaged total electric field of the co-rotating 95 GHz  $TE_{6,2}$  and  $TE_{10,1}$  modes, respectively [17]. In Fig. 4, the experimental phase pattern of the co-rotating 140 GHz  $TE_{28,8}$  mode is plotted (left), generated by a specific low-power mode generator (see Section 5) and measured using a standard rectangular waveguide probe antenna [18]. Along an azimuthal circle, 27 phase spirals can be counted (right). In the center of the pattern the phase is random because the very small  $E_r$  and  $E_\phi$  fields.

All the phase patterns presented in Figs. 3 and 4 show  $m-1$  phase spirals, which means that the OAM mode number of co-rotating  $TE_{m,n}$ -gyrotron modes is  $l = m-1$ . The mode number of the TAM is  $m = l + 1$ . The SAM with  $s = 1$  has the same sense of rotation as the OAM. For counter-rotating modes the signs are reversed.

Tab. 2 Intensity on axis  $I_0$ , spin angular momentum (SAM) and orbital angular momentum (OAM) of rotating gyrotron TE modes in circular waveguides.

Mode Family	$I_0$ (Intensity on Waveguide Axis)	SAM (Circular Polarization)	OAM
$TE_{0,n}$	no (Annual Intensity Pattern)	no ( $s = 0$ )	no ( $l = 0$ )
$TE_{l,l}$	yes	yes ( $s = 1$ ) only RHCP	no ( $l = 0$ )
$TE_{l,n} (n > 1)$	yes	yes ( $s = \pm 1$ )	no ( $l = 0$ )
$TE_{m,l} (m > 1)$ WGM	no (Annual Intensity Pattern)	yes ( $s = 1$ ) only RHCP	yes ( $l = m - 1$ )
$TE_{m,n} (m, n > 1)$	no (Annual Intensity Pattern)	yes ( $s = \pm 1$ )	yes ( $\pm l = \pm m \mp 1$ )

Table 1 summarizes the SAM and OAM features of different types of gyrotron TE modes. A special case are the circular symmetric modes ( $m = 0$ ), where the optimum electron beam radii  $R_b$  for excitation of “co- and counter-rotating modes” are identical (radius of electric field maximum, see eqs. 6 and 7). Here  $m = l + s = 0$ , with no rotation ( $l = 0$ , no OAM), and since the electric field



is at each transverse coordinate linearly polarized:  $s = 0$  (no SAM). The circularly polarized  $TE_{l,l}$  mode has  $s = 1$  (RHCP) and  $l = 0$ . Circularly polarized (rotating)  $TE_{l,n}$  modes ( $n > 1$ ) show a SAM ( $s = \pm 1$ ) but have no OAM ( $l = 0$ ). In the case of whispering gallery modes  $TE_{m,l}$  modes (WGMs) with  $m > 1$ , only the co-rotating modes can be excited, since always  $\chi_{m+1,l} > \chi_{m,l}$  (see eq. 7). Co-rotating  $TE_{m,n}$  gyrotron modes with  $m, n > 1$  have the OAM mode number  $l = m - 1$  (number of phase spirals) and SAM ( $s = 1$ ), since their electric fields are at each transverse coordinate circularly polarized with the same sense of rotation. For counter-rotating (LHCP) modes the signs are reversed.

From the above considerations follows:

**For possible applications of gyro-devices in long-range wireless communication with OAM diversity, the  $TE_{2,2}$  mode is the lowest order OAM mode, carrying the topological charges  $l = \pm 1$ , depending whether it is co- or counter-rotating with respect to the electron gyration in the cavity magnetic field.**

#### 4. Gyrotron orbital angular momentum beam transmitters

Current megawatt-class high-power gyrotrons for electron cyclotron heating, non-inductive current drive, and collective Thomson scattering diagnostics in magnetically confined thermonuclear fusion plasmas are equipped with highly efficient quasi-optical output couplers, which convert the rotating very-high-order  $TE_{m,n}$ -cavity mode to a fundamental, linearly polarized Gaussian output beam with transversal tube output window [13, 14, 15, 19]. Of course, the output of future gyrotron OAM beam transmitters must not use such output mode converters. In this case, directly the rotating interaction circuit mode should be used as tube output through an axially installed dielectric window [20].

Since propagation of higher-order OAM beams in free space results in large diffraction angles, a mode-conserving, non-linear waveguide diameter up-taper section should be added after the interaction circuit to reduce the Brillouin angle  $\theta_B$  of the output wave. In addition, focusing lenses should be installed to reduce beam diffraction.

Several today's Ku/Ka-band 10-to-30-*kW*-class gyrotrons for various technological and industrial applications operate in a low-order rotating cavity mode, e.g.  $TE_{2,2}$ ,  $TE_{3,2}$ , or  $TE_{2,3}$ , which also serves as axial (longitudinal) output mode [13]. Such tubes could be used for high-power OAM techniques. In the early 1990-ties, the Research Center Karlsruhe (FZK, now KIT) and several vacuum electron tube companies performed very successful experiments with 0.5 – 1.0 *MW*-class axial output gyrotrons. Those operated in the following OAM modes [13]:

84 GHz, 110 GHz and 140 GHz,  $TE_{15,2}$  (VARIAN, now CPI),

110 GHz,  $TE_{12,2}$  and  $TE_{22,2}$  (VARIAN, now CPI),

110 GHz,  $TE_{6,4}$  (THOMSON, now THALES),

120 GHz,  $TE_{12,2}$  and  $TE_{22,12}$  (JAERI, TOSHIBA, now QST, CANON)

140 GHz,  $TE_{10,4}$  and  $TE_{28,16}$  (FZK, now KIT),

165 GHz,  $TE_{31,17}$  (FZK, now KIT).

The output of such gyrotrons could be used for long-range wireless communication with OAM diversity. Provided that the tube is equipped with a triode-type magnetron injection electron gun (MIG) with modulation anode and that it operates with suitable electron beam radius  $R_b$ , it may be electronically switched between the co- and counter-rotating cavity modes (right- and left handed OAM) at the same operating frequency. To achieve high frequency stability and a narrow line width, a phase locking system can be utilized to control the electron beam energy. The long-term stability can be guaranteed by a reference clock. The relative width of the frequency spectrum and the frequency stability obtained of a 263 GHz, 100 W gyrotron, operating in the  $TE_{5,3}$ -cavity mode are  $4 \cdot 10^{-12}$  (approximately 1 Hz line width!) and  $10^{-10}$ , respectively [21].

#### **4.1. KIT 500 kW, 140 GHz $TE_{10,4}$ mode gyrotron with axial output**

This tube was equipped with a non-linear up-taper from the cavity (16.22 mm diameter) to the 70 mm diameter output waveguide which also served as collector. The tube output was through a



Fig. 5 Measurement of the mode purity of a  $TE_{10,4}$ -mode gyrotron using a wavenumber spectrometer.

frequency tunable double-disk FC75 face cooled sapphire window. The measured electronic efficiency of was 31 % (without depressed collector) [22]. High-power measurements of the output mode content using a 70 mm diameter wavenumber spectrometer (see Fig. 5) [23] resulted in a purity of the co-rotating  $TE_{10,4}$  output mode of better than 98 % (wrong mode content < -17 dB).

#### 4.2. KIT 1.2 MW, 165 GHz $TE_{31,17}$ mode coaxial-cavity gyrotron with axial output

In coaxial gyrotron cavities the existence of the longitudinally-corrugated inner rod reduces the problems of mode competition and limiting current, thus allowing one to use even higher order modes at 2 MW power level with the same Ohmic attenuation as in 1 MW-class cylindrical cavities [24]. Successful activities on the development of 1.5 – 2 MW short-pulse gyrotrons with coaxial cavities and axial output window were conducted at IAP Nizhny Novgorod ( $TE_{28,16}$  - mode at 140 GHz [25]) and KIT (FZK) Karlsruhe (modes  $TE_{28,16}$  at 140 GHz and  $TE_{31,17}$  at 165 GHz) [24, 26]. In preliminary 1 ms short pulse operation of the 165 GHz tube with  $R_0 = 27.38$  mm cavity radius and  $R_b = 9.57$  mm electron beam radius, at  $B = 6.61$  T,  $V_b = 84.8$  kV and  $I_b = 52$  A, a maximum RF output power in the co-rotating  $TE_{31,17}$ -mode (OAM state  $l = 30$ ) as

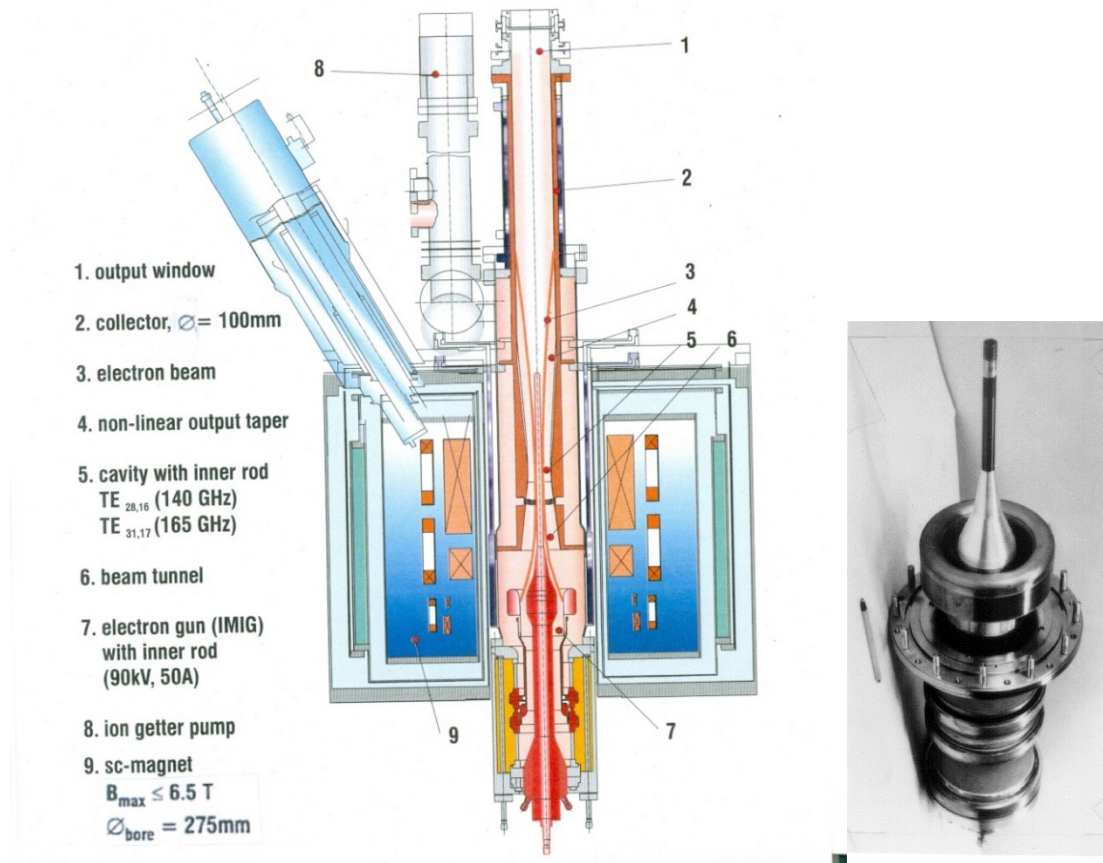


Fig. 5 Schematic of the 1.7 MW 165 GHz  $TE_{31,17}$ -mode gyrotron with coaxial cavity (left), inverse magnetron injection electron gun (right) and axial output through a 100 mm diameter collector waveguide and window [27].

high as  $1.2\text{ MW}$  was achieved with an efficiency of  $27\%$  [27]. In this gyrotron cavity the co-rotating  $\text{TE}_{90,1}$  mode at  $163.4\text{ GHz}$  would have the highest OAM state number ( $l = 89$ ). Fig. 6 shows a schematic of this gyrotron in its superconducting magnet and a photo of the utilized inverse magnetron injection gun (IMIG). For mode purity measurements, an optimized, non-linear taper to a waveguide diameter of  $140\text{ mm}$  was installed after the  $100\text{ mm}$  diameter output window.

The calculated near-field pattern of the non-rotating  $\text{TE}_{31,17}$ -mode at the up-taper output is shown in Fig. 6. In Fig. 7, the corresponding pattern of the calculated rotating mode is plotted, the horizontal polarization (left) and the vertical polarization (right). The complete measured near-field pattern of the rotating mode, recorded at high power using a PVC target plate and an infrared camera, is shown in Fig. 8. The measured high-power far-field pattern of the co-rotating  $\text{TE}_{31,17}$ -mode is plotted in Fig. 9. A teflon lens at the up-taper output ( $140\text{ mm}$  diameter), with a focal length of  $165\text{ mm}$ , made the far-field transformation. Fig. 10 shows the measured far-field pattern of the co-rotating  $\text{TE}_{31,17}$ -mode [27], where some counter-rotating mode was generated intentionally by means of reflection at a longitudinal quartz plate on the axis of propagation. In azimuthal direction, 62 intensity maxima and minima can be counted (see also Fig. 6).

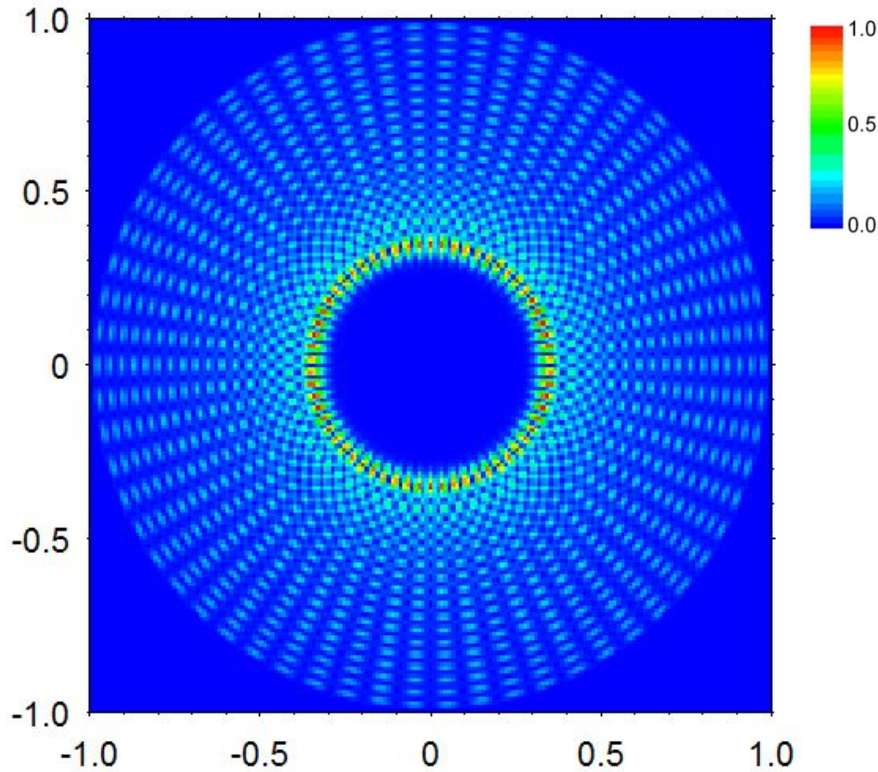


Fig. 6 Calculated near-field pattern of the non-rotating  $\text{TE}_{31,17}$ -mode at the up-taper output ( $140\text{ mm}$  diameter). The caustic radius is  $R_c = 22.9\text{ mm}$ .

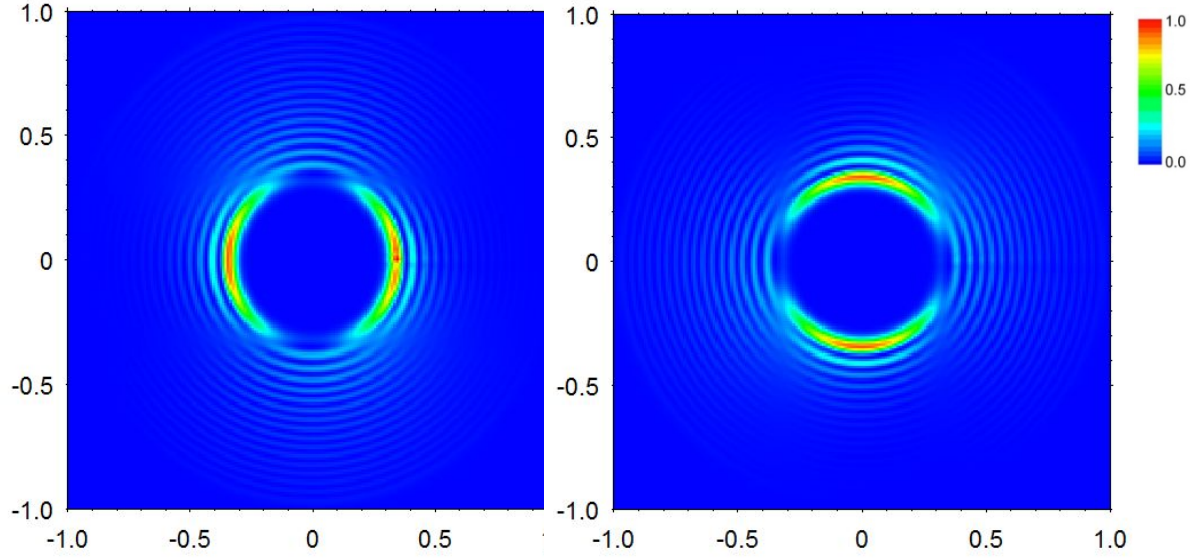


Fig. 7 Calculated near-field pattern of the co-rotating  $TE_{31,17}$ -mode ( $l = 30$ ) at the up-taper output (140 mm diameter). The caustic radius is  $R_c = 22.9$  mm. Horizontal polarization (left), vertical polarization (right).

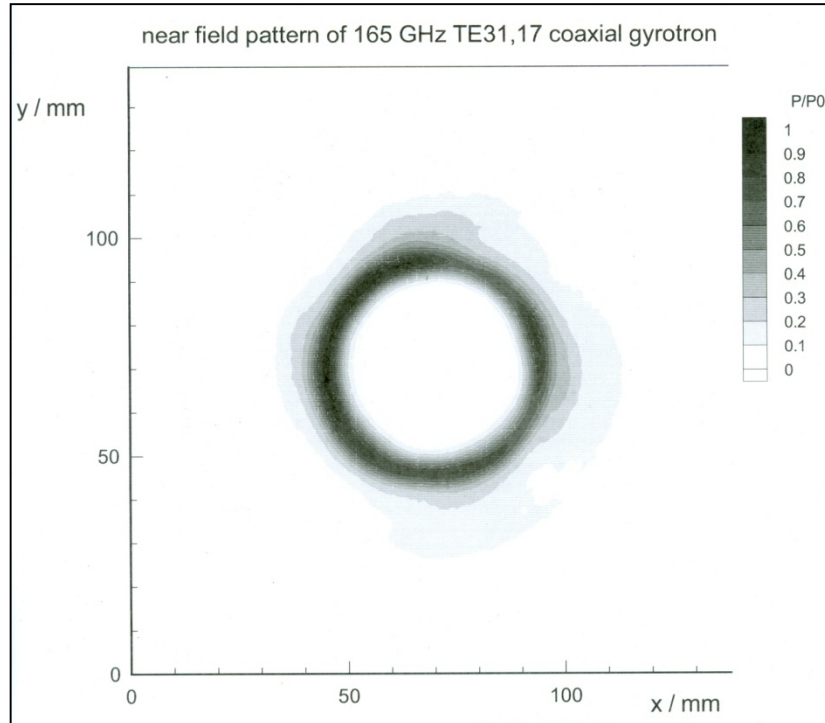


Fig. 8 Measured high-power near-field pattern of the co-rotating 165 GHz  $TE_{31,17}$ -mode with OAM state number  $l = 30$  at the up-taper output (140 mm diameter). The caustic radius is  $R_c = 22.9$  mm.



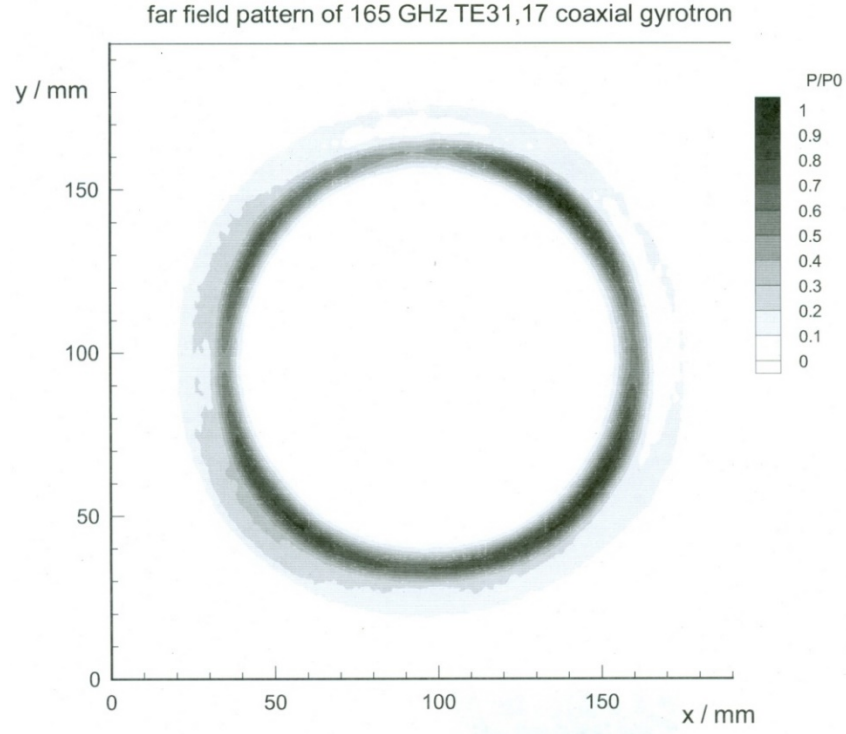


Fig. 9 Measured high-power far-field pattern of the co-rotating 165 GHz  $TE_{31,17}$ -mode with OAM  $l = 30$ . A teflon lens with a focal length of 165 mm at the up-taper output (140 mm diameter) performed the far-field transformation.

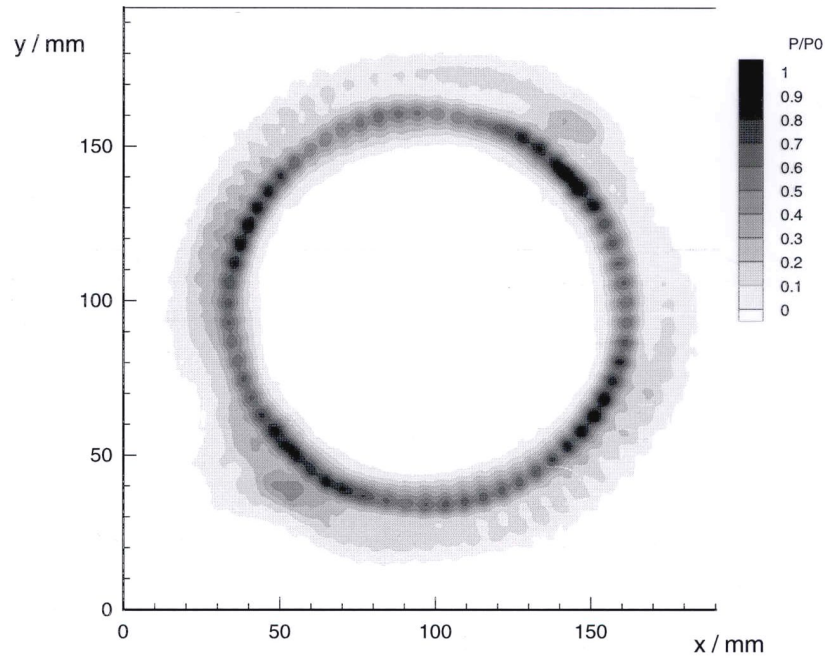


Fig. 10 Measured high-power far-field pattern of the co-rotating 165 GHz  $TE_{31,17}$ -mode, where some counter-rotating mode was intentionally produced by means of reflection at a quartz plate, positioned longitudinally on the axis of propagation [27]. In azimuthal direction, 62 intensity maxima and minima can be counted (see Fig. 6).

### 4.3. Gyro-Amplifiers

As shown in Table 1, the family of gyro-devices also consists of different types of amplifiers, the gyro-klystron with a bandwidth  $< 1\%$ , the gyro-twystron with  $\approx 2\%$  bandwidth and the gyro-traveling-wave tube (gyro-TWT) providing  $\approx 10\%$  bandwidth [13]. Such amplifiers could be used for long-range wireless communications with OAM diversity. Due to mode competition with absolute instable back-ward waves, mostly very low order modes are employed in the interaction circuits of these amplifiers e.g.  $TE_{1,1}$  or  $TE_{0,1}$ , which cannot be used for OAM applications (see Table 2). Nevertheless, there are a few investigations on higher-order mode devices, as e.g. the 2<sup>nd</sup> harmonic 31.8 GHz inverted gyro-twystron of NRL Washington D.C. operating in the  $TE_{4,2}$  mode ( $l = \pm 3$ ), with 160 kW output power at 25 % efficiency, 33 dB gain, and 1.3 % bandwidth [28]. Further investigation on such devices is needed in order to develop broadband amplifiers for OAM communications.

## 5. Mode and Helical Wavefront Selective Gyrotron OAM Beam Receivers

Application of rotating high-order OAM gyrotron modes in long-range wireless communication systems requires corresponding mode and helical wavefront sensitive detectors for selective OAM-mode sorting, which are described in the present section. The first needed components are beam splitters with low crosstalk to provide the necessary receiver channels, which are matched to right and left - hand rotation of the utilized OAM modes (de-multiplexer). For a number of  $x$  OAM modes,  $2x$  receiver channels with  $2x-1$  beam splitters are required. Those can be realized in oversized circular waveguide or quasi-optical techniques [29, 30, 31], which is also the case for the mode and helical wavefront selective detector channels [32]. At low power levels, in long-range applications, spiral phase plates (SPPs), holographic diffraction gratings, birefringent liquid crystals, spiral reflectors, specific array antennas, and anisotropic frequency selective surfaces (meta-surfaces) [8, 9, 10, 11, 12, 33 and references given there] can be used. In the present report, oversized circular waveguide and quasi-optical techniques are discussed, which can be used at higher power levels.

### 5.1. OAM selective oversized waveguide detection systems

Oversized waveguide OAM mode sorting and detection systems are based on sequences of periodic perturbed-wall mode converters for rotating modes [34, 35, 36, 37, 38]. In overmoded circular waveguides with average radius  $a_0$  a selective transformation of one specific mode with azimuthal mode index  $m_1$  into another mode with azimuthal index  $m_2$  can be achieved by means of a periodic helical structure ( $\Delta m \cdot \varphi - \Delta \beta \cdot z = \text{const.}$ ) of the inner waveguide wall:

$$a(z, \varphi) = a_0 + a_1 \cos(\Delta m \cdot \varphi - \Delta \beta \cdot z) \quad (13)$$

under the condition that the geometric period  $\lambda_w$  of the wall perturbations and the unperturbed wavenumbers  $\beta_1$  and  $\beta_2$  of the interacting modes have to satisfy the resonance relationship

$$\Delta\beta = \beta_1 - \beta_2 = 2\pi / \lambda_B = 2\pi / \lambda_w \quad (14)$$

and

$$\pm \Delta m = m_1 - m_2 \quad (15)$$

where  $\lambda_B = \lambda_1 \lambda_2 / (\lambda_2 - \lambda_1)$  is the beat wavelength of the two modes. The radial wavenumber of the mode is changed by scattering the incoming wave at the periodic structure of the waveguide wall which acts as a diffraction grating. Fourier integral transformation theory yields the general conclusion, that the length of the mode converter must be at least of the order of  $\lambda_B$  of the two considered modes. The coherence condition (14) guarantees that the conversion to other unwanted modes, which are also coupled by the waveguide perturbations (same  $\Delta m$ ), suffers destructive interference. The requirements for low parasitic mode amplitudes are  $\Delta\beta \neq \beta_{1,2} - \beta_p$  or  $\Delta m \neq m_{1,2} - m_p$ , where  $\beta_p$  is the wavenumber and  $m_p$  the azimuthal mode index of the parasitic mode. Mode transformers consisting of a large number  $N$  of geometrical periods create low levels of unwanted parasitic modes but inherently exhibit narrow bandwidth [39].

Here, as an example, the four-step mode conversion series  $TE_{12,2}$  (right-hand rotating) –  $TE_{0,6}$  –  $TE_{0,4}$  –  $TE_{0,1}$  –  $TE_{1,0}$  (standard rectangular w.g.) at 120 GHz and average waveguide radius  $a_0 = 8.74$  mm (waveguide type designation C120) will be described [36, 38]. Table 3 summarized the geometrical parameters of the helical (corkscrew-type) mode converter of the first-step. It consists of 3 periods, where the first and third sections are equipped with linear perturbation amplitude tapers (see Fig.11). The two-step conversion  $TE_{0,6}$  –  $TE_{0,4}$  –  $TE_{0,1}$  can be done employing highly efficient (98 %) circular symmetric, periodically rippled wall mode transducers [40]. Finally, the  $TE_{0,1}$  –  $TE_{1,0}$  (standard rectangular w.g.) conversion can be performed by using adiabatic King-type, Southworth-type or Marié-type transducers [20].

Tab. 3 Geometrical parameters of helical 120 GHz  $TE_{12,2}$  (right-hand rotating) –  $TE_{0,6}$  mode converter in circular waveguide with average radius  $a_0 = 8.74$  mm (waveguide norm C120) [36] (mechanical tolerances are  $< 0.01$  mm).

Type of Mode Converter at 120 GHz	$TE_{12,2}$ to $TE_{0,6}$
Difference of Azimuthal Mode No. $\Delta m$	12
Maximum Perturbation Amplitude $a_1$	0.074 mm
Wall Period Length $\lambda_w$	36.597 mm
Number of Periods $N$	3 (2 periods are tapers)
Total Length $L$	109.79 mm
Output Mode Purity	99.9 %
Ohmic Losses	1.4 %



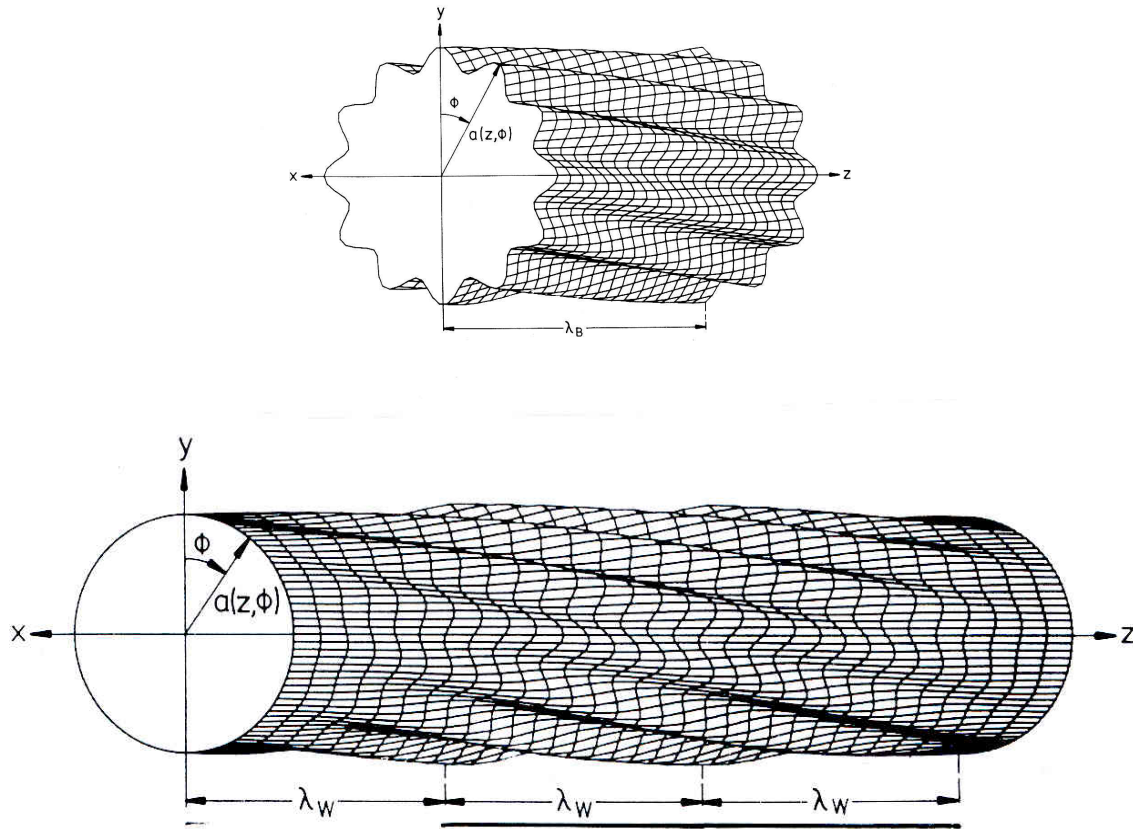


Fig. 11 Schematic of the right-hand helical, corkscrew-type  $TE_{12,2}$ -to- $TE_{0,6}$  mode converter wall contour, including linearly tapered input and output sections [36].

## 5.2 OAM selective quasi-optical detection systems

Rotation sensitive quasi-optical OAM mode sorting and detection systems are based on quasi-optical mode converters, as they are used in high-power fusion gyrotrons [32], or on mode generators for rotating higher-order modes [41, 42]. Figure 12 shows the photo of such a mode generator [43]. It consists of a Gaussian mode launching horn antenna, fed by a standard rectangular waveguide, a system of cylindrical lenses for proper beam shaping, a quasi-parabolic cylindrical mirror and a gyrotron-type coaxial cavity with perforated, translucent wall for excitation of the desired high-order mode. The correct sense of rotation is achieved by optimized launching of the microwave beam through the cavity-wall perforation to the caustic radius of the desired rotating mode [18, 44]. Of course, for OAM mode detection, this arrangement would be used the other way round. Careful alignment of such a mode generator system leads to suppression of mode power with the wrong sense of rotation by 23 dB. The highest-order mode, which has been generated using such a system, is the  $TE_{40,23}$  mode at 204 GHz [18].

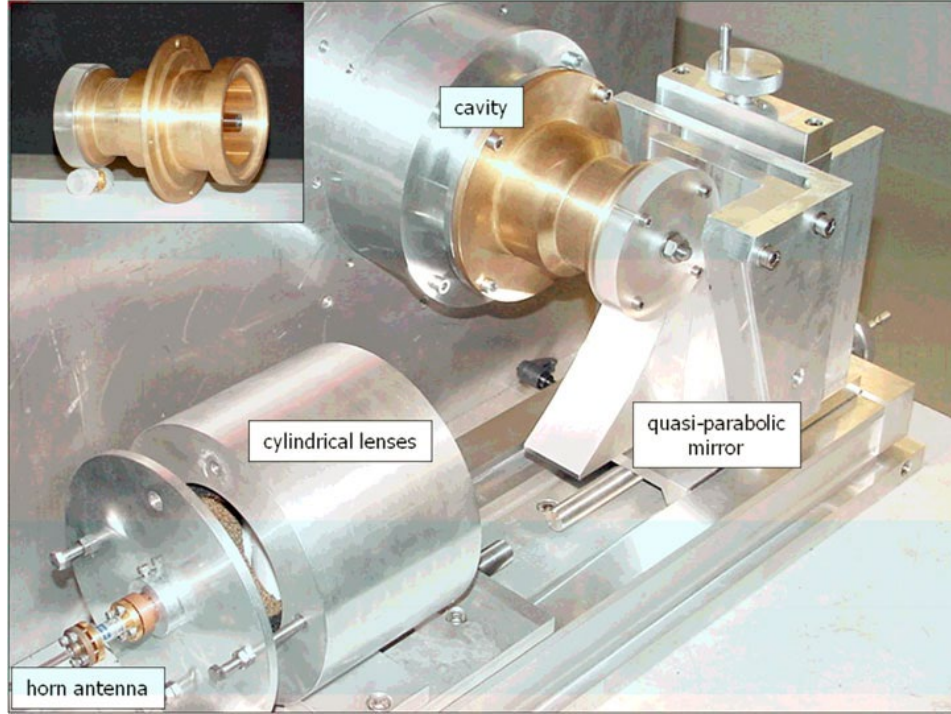


Fig. 12 Photo of a quasi-optical mode generator for rotating high-order gyrotron-type modes [43].

## 6. Conclusions

The orbital angular momentum (OAM) of electromagnetic-wave beams provides further diversity to multiplexing in wireless communication. The present paper shows that higher-order mode gyrotron oscillators and gyro-amplifiers are natural sources of very pure high-power high-order OAM millimeter (*mm*) wave beams. The well-defined total angular momentum (TAM) of rotating gyrotron modes operating close to the cutoff frequency of the cylindrical interaction circuit can be derived by photonic and electromagnetic (EM) wave approaches. Rotating (circularly polarized)  $TE_{m,p}$  modes exhibit the TAM mode number  $m$  where  $m = l + 1$ . Their OAM with mode number (topological charge)  $l = m - 1$  ( $|l|$  spirals of the helical phase pattern), and spin angular momentum (SAM) with  $s = 1$  have the same sense of rotation. Such very pure OAM mm-wave beams generated by gyro-devices with axial output in the operating mode of the interaction circuit (no internal mode converter) could be used for long-range wireless communication with OAM diversity. Corresponding mode and helical wavefront sensitive detectors for selective OAM-mode sorting can be realized in oversized circular waveguide or quasi-optical beam waveguide technologies. The rotating  $TE_{2,2}$  mode is the lowest order OAM mode, carrying the topological charges  $l = \pm 1$ , depending whether it is co- or counter-rotating with respect to the electron gyration in the longitudinal magnetic field of the interaction circuit in the gyro-device.

## Acknowledgments

The author wishes to express his deep gratitude to EunMi Choi and Ashwini Sawant from Ulsan National Institute of Science and Technology (UNIST), Ulsan, South Korea, for the fruitful and excellent collaboration in this field of gyrotron OAM modes, starting from his two-month stay in 2015 as Visiting Professor at UNIST. In addition, he would like to thank Dietmar Wagner from Max-Planck-Institute for Plasma Physics, Garching, Germany, for calculating the mode patterns shown in Figures 6 and 7 as well as Stefan Illy and Tobias Ruess, KIT, for very fruitful discussions on rotating gyrotron modes and quasi-optical OAM mode detectors. Finally, the author is very glad to acknowledge the help of Oliver Braz, EnNet GmbH, Wemding, Germany, and Vladimir Malygin, Institute of Applied Physics (IAP) of the Russian Academy of Sciences (RAS), Nizhny Novgorod, Russia, who performed in 1998 the high-power near- and far-field measurements of the rotating gyrotron  $TE_{31,17}$ -mode plotted in Figures 8 and 9, working as PhD student, respectively visiting scientist in the Karlsruhe Gyrotron Team. Regrettably, V. Malygin passed away on April 12, 2019.

## References

- [1] F.J. Belinfante. "On the current and the density of the electric charge, the energy, the linear momentum and the angular momentum of arbitrary fields". *Physica*, 7, No. 5, 449-474 (1940).
- [2] J.H. Poynting. "The wave motion of a revolving shaft, and a suggestion as to the angular momentum in a beam of circularly polarized light". *Proc. Royal Society London A*, 82, 560-567 (1909).
- [3] R. Beth. "Mechanical detection and measurement of the angular momentum of light". *Phys. Rev.*, 50, 115-125 (1936).
- [4] L. Allen, M.W. Beijersbergen, R.J.C. Spreeuw, et al. "Orbital angular momentum of light and the transformation of Laguerre-Gaussian laser modes". *Phys. Rev. A*, 435, 8185-8189 (1992).
- [5] J. Wang, J.-Y. Yang, I.M. Fazal, et al. "Terabit free-space data transmission employing orbital angular momentum multiplexing". *Nature Photonics*, 6, 488-496 (2012).
- [6] S. Franke-Arnold, L. Allen, and M. Padgett. "Advances in optical angular momentum". *Laser Photon. Rev.*, 2, 299-313 (2008).
- [7] A.M. Yao and M.J. Padgett. "Orbital angular momentum, origins, behavior and applications". *Adv. Opt. Photon.*, 3, 161-204 (2011).
- [8] J. Yang, C. Zhang, H.F. Ma, et al. "Generation of radio vortex beams with designable polarization using anisotropic frequency selective surface". *Appl. Phys. Lett.*, 112, 203501 (5pp) (2018).
- [9] H. Shi, L. Wang, X. Chen, et al. "Generation of a microwave beam with both orbital and spin angular momenta using a transparent metasurface". *J. Appl. Phys.*, 126, 063108 (7pp) 2019.
- [10] R.M. Henderson. "Let's do the twist!". *IEEE Microwave Magazine*, 6, 88-96 (2017).

- [11] M. Veysi, C. Guclu, F. Capolino, et al. "Revisiting orbital angular momentum beams". *IEEE Antennas & Propagation Magazine*, 4, 68-81 (2018).
- [12] Y. Yan, G. Xie, M.P.J. Lavery, et al. "High-capacity millimeter-wave communications with orbital angular momentum multiplexing". *Nature Communications*, 5, 4876 (8pp) (2014).
- [13] M. Thumm. "State-of-the-art of high-power gyro-devices and free electron masers". *J. Infrared, Millimeter, and Terahertz Waves*, doi.org/ 10.1007/s10762-019-00631-y.
- [14] G.S. Nusinovich, M.K.A. Thumm, and M.I. Petelin. "The gyrotron at 50: Historical Overview". *J. Infrared, Millimeter, and Terahertz Waves*, 35, 325-381 (2014).
- [15] M.V. Kartikeyan, E. Borie, and M. Thumm. "*Gyrotrons – High Power Microwave and Millimeter Wave Technology*". Springer, Berlin, Germany, ISBN 3-540-40200-4, 2004.
- [16] A. Sawant, M.S. Choe, M. Thumm, et al. "Orbital angular momentum (OAM) of rotating modes driven by electrons in electron cyclotron masers". *Scientific Reports*, 7, 3373 (10pp) (2017).
- [17] M. Thumm, A. Sawant, M.S. Choe, et al. "The gyrotron – A natural source of high-power orbital angular momentum millimeter-wave beams". *EPJ Web of Conferences*, 149, 04014 (2pp) (2017).
- [18] T. Ruess, K.A. Avramidis, G. Gantenbein, et al. "Computer-controlled test system for the excitation of very high-order modes in oversized waveguides". *J. Infrared, Millimeter, and Terahertz Waves*, 40, 257-268 (2019).
- [19] M.K.A. Thumm, G.G. Denisov, K. Sakamoto, et al. "High-power gyrotrons for electron cyclotron heating and current drive". *Nuclear Fusion*, 59, 073001 (37pp) (2019).
- [20] M. Thumm. "Modes and mode conversion in microwave devices". in *Generation and Application of High Power Microwaves*, R.A. Cairns and A.D.R. Phelps, eds., Institute of Physics Publishing, Bristol and Philadelphia, 121-171 (1997).
- [21] A. Fokin, M. Glyavin, G. Golubiatnikov, et al. "High-power sub-terahertz source with a record frequency stability at up to 1 Hz". *Scientific Reports*, 8, 4317 (6pp) (2018).
- [22] G. Gantenbein, E. Borie, G. Dammertz, et al. "Experimental results and numerical simulations of a high power 140 GHz gyrotron". *IEEE Trans. on Plasma Science*, 22, 861-870 (1994).
- [23] W. Kasparek and G. Müller. "The wavenumber spectrometer". *Int. J. Electronics*, 64, 5-20 (1988).
- [24] B. Piosczyk, G. Dammertz, O. Dumbrajs, et al.. "165 GHz coaxial cavity gyrotron". *IEEE Trans. on Plasma Science*, 32, 853-860 (2004).
- [25] V.E. Zapevalov, A.B. Pavelyev, and V.I. Khizhnyak. "Natural scheme of electron beam energy recovery in a coaxial gyrotron". *Radiophysics and Quantum Electronics*, 43, 671-674 (2000)
- [26] B. Piosczyk, O. Braz, G. Dammertz, et al. "A 1.5-MW, 140-GHz, TE<sub>28,16</sub>-coaxial cavity gyrotron". *IEEE Trans. on Plasma Science*, 25, 460-469 (1997).
- [27] C.T. Iatrou, O. Braz, G. Dammertz, et al. "Design and experimental operation of a 165-GHz, 1.5-MW, coaxial-cavity gyrotron with axial rf output". *IEEE Trans. on Plasma Science*, 25, 470-479 (1997).
- [28] H. Guo, S.H. Chen, V.L. Granatstein, et al. "Operation of a highly overmoded, harmonic-multiplying, wideband gyrotron amplifier". *Phys. Rev. Letters*, 79, 515-518 (1997).

- [29] S.V. Kuzikov, G.G. Denisov, M.I. Petelin, et al. "Study of Ka-band components for a future high-gradient accelerator". *Proc. Int. Workshop Strong Microwaves in Plasmas*, ed. A.G. Litvak, Nizhny Novgorod, Vol. 1, 255-263 (2003).
- [30] A.A. Bogdashov, G.G. Denisov, S.V. Samsonov, et al. "High-power Ka-band transmission line with a frequency bandwidth of 1 GHz". *Radiophysics and Quantum Electronics*, 58, 777-788 (2016).
- [31] M. Petelin, V. Erckmann, J. Hirshfield, et al. "New concepts for quasi-optical structures for use with gyrotron systems". *IEEE Trans. on Electron Devices*, 56, 835-838 (2009).
- [32] M. Thumm and W. Kasperek. "Passive high-power microwave components". *IEEE Trans. on Plasma Science*, 30, 755-786 (2002).
- [33] G. Junkin, J. Parrón, and A. Tennant. "Characterization of an eight-element circular patch array for helical beam modes". *IEEE Trans. on Antennas and Propagation*, 67, 7348-7355 (2019).
- [34] J.L. Doane. "Polarization converters for circular waveguide modes". *Int. J. Electronics*, 61, 1109-1133 (1986).
- [35] P. Garin, E. Jedar, G. Jendrzczak, et al. "Symmetric and non-symmetric modes in a 200 kW, 100 GHz gyrotron". *Conf. Digest 12<sup>th</sup> Int. Conf. on Infrared and Millimeter Waves*, Lake Buena Vista (Orlando), Florida, USA, 194-195 (1987).
- [36] M. Thumm and A. Jacobs. "In-waveguide  $TE_{0,1}$ -to-whispering gallery mode conversion using periodic wall perturbations". *Conf. Digest 13<sup>th</sup> Int. Conf. on Infrared and Millimeter Waves*, Honolulu, Hawaii, USA, 465-466 (1988).
- [37] M. Thumm, A. Jacobs, and J. Pretterebner. "Generation of rotating high-order  $TE_{m,n}$  modes for cold-test measurements on high-power quasi-optical gyrotron output mode converters". *Conf. Digest 15<sup>th</sup> Int. Conf. on Infrared and Millimeter Waves*, Orlando, Florida, USA, 204-206 (1990).
- [38] Iima, M., M. Sato, J. Amano, et al. "Measurement of radiation field from an improved efficiency quasi-optical converter for whispering-gallery mode". *Conf. Digest 14<sup>th</sup> Int. Conf. on Infrared and Millimeter Waves, Proc., SPIE*, 1240, Würzburg, Germany, 405-406 (1989).
- [39] M. Thumm. "High power mode conversion for linearly polarized  $HE_{11}$  hybrid mode output". *Int. J. Electronics*, 61, 1135-1153 (1986).
- [40] H. Kumric, M. Thumm, and R. Wilhelm. "Optimization of mode converters for generating the fundamental  $TE_{01}$  mode from  $TE_{06}$  gyrotron output at 140 GHz". *Int. J. Electronics*, 64, 77-94 (1988).
- [41] N.L. Aleksandrov, A.V. Chirkov, G.G. Denisov, et al. "Selective excitation of high-order modes in circular waveguides". *Int. J. Infrared and Millimeter Waves*, 13, 1369-1385 (1992).
- [42] M. Pereyaslavets, O. Braz, S. Kern, et al. "Improvements of mode converters for low-power excitation of gyrotron-type modes". *Int. J. Electronics*, 82, 107-115 (1997).
- [43] T. Rzesnicki, J. Jin, B. Piosczyk, et al. "Low power measurements on the new RF output system of a 170 GHz, 2 MW coaxial cavity gyrotron". *Int. J. Infrared and Millimeter Waves*, 27, 1-11 (2006).
- [44] T. Ruess, K.A. Avramidis, M. Fuchs, et al. "Towards fully automated systems for the generation of very high order modes in oversized waveguides". *EPJ Web of Conferences*, 195, 01030 (2pp) (2018).